Wrexham University Research Online

Journal Article

Machine Learning-Assisted Microstrip Antenna Design Featuring Extraordinary Polarization Purity

Rafidul, S., Akinsolu, M. O. Akinsolu, Liu, B. Liu, Kumar, C. and Guha, D.

This article is published by IEEE. The definitive version of this article is available at:
https://ieeexplore.ieee.org/abstract/document/10818774

Recommended citation:

Rafidul, S., Akinsolu, M. O. Akinsolu, Liu, B. Liu, Kumar, C. and Guha, D. (2025), 'Machine Learning-Assisted Microstrip Antenna Design Featuring Extraordinary Polarization Purity,' in IEEE Antennas and Wireless Propagation Letters, vol. 24, no. 4, pp. 1008-1012, April 2025. doi: 10.1109/LAWP.2024.3524249.

Machine Learning-Assisted Microstrip Antenna Design Featuring Extraordinary Polarization Purity

Sk Rafidul, *Member, IEEE*, Mobayode O. Akinsolu, *Senior Member, IEEE*, Bo Liu, *Senior Member, IEEE*, Chandrakanta Kumar, *Senior Member, IEEE*, and Debatosh Guha, *Fellow, IEEE*

***Abstract*—A high degree of polarization purity for microstrip antennas has been successfully explored. This, to the best of our knowledge, is the first of its kind and claims a twofold novelty: a stepwise development of complex multiunit defected ground geometry (DGG) based on a thorough scientific analysis and use of a machine learning-assisted global antenna optimization method, particularly, the parallel surrogate model-assisted hybrid differential evolution for antenna synthesis (PSADEA) algorithm, which is often more than ten times faster than popular global optimization techniques, while obtaining superior results. They result in highly optimal solutions considering multiple performances, i.e., reduction in cross-polarization (XP) radiations simultaneously over orthogonal (H-) and diagonal (D-) planes maintaining the primary gain unaffected. The proposed DGG has been satisfactorily tested with different patches and arrays fabricated in C band. Typically, 7.5 dBi to 8.0 dBi peak gain has been ensured along with 13 dB to 18 dB improvement in XP level over entire radiation planes. A 4-element array on an identical DGG promises over 40 dB co-to-XP isolation over the entire azimuth planes.**

***Index Terms*—Artificial intelligence, ground plane engineering, machine learning, microstrip antenna, polarization purity.**

I. Introduction

OPTIMAL signal transmission/reception by microstrip antennas hinges on maintaining polarization purity as a top priority [1], [2]. Although it naturally exhibits outstanding polarization purity in its E-plane (azimuth $\varphi = 0°$), the situation dramatically changes over the H- ($\varphi = 90°$) and diagonal ($\varphi = 45°$ or D-) planes [3]. Several earlier endeavors explored engineering with feed [4], [5], [6], [7]; patch and layers [7], [8], [9], [10]; and ground plane (GP) [11], [12], [13], [14], [15], [16], [17] to mitigate the cross-polarization (XP) issue, especially across H-plane. However, it is more serious and equally challenging across D-planes [3]. A few studies [18], [19], [20] and [21] have recently addressed it, of which [20] and [21] compromised with the H-plane performance and the rest [18], [19] encountered limitations in realizing arrays.

The present investigation aims to alleviate all these shortcomings. A multi-Parametric defected ground geometry (DGG) has been introduced. Its complexity, along with multiple challenging goals (lowering XP on both D- and H-planes and maintaining the gain unaltered), makes the problem complex. Simple analysis or manual tuning thus becomes next to impossible to predict the optimum DGG solution.

Popular global optimization techniques [e.g., differential evolution (DE) and particle swarm optimization (PSO)] are not suitable due to suboptimal solutions and long optimization times. The present work, therefore, leans towards a machine learning (ML)-assisted global optimization method, more specifically, *parallel surrogate model-assisted hybrid differential evolution for antenna synthesis* (PSADEA) method [22], [23]. This method is often more than ten times faster than DE and PSO and is much superior in handling complex antenna structures considering the obtained design solution quality [22], [23].

The step-by-step development and design physics are discussed in the following sections. The newly proposed DGG has been tested with varying microstrip shapes and arrays. The fabricated C-band prototypes measuring $1\lambda \times 0.9\lambda \times 0.03\lambda$ offer about 4% to 5% impedance bandwidth, 7.5 dBi to 8.0 dBi peak gain along with 87% to 91% radiation efficiency. They ensure 13 dB to 18 dB improvement in XP level over entire radiation planes for all patch shapes. A 2×2 C-band rectangular patch array (element spacing 0.5λ in E-plane and 0.57λ in H-plane) also ensures more than 40 dB co-to-XP isolation over entire azimuth planes.

II. New Geometry: Conjecture and Development

With reference to Fig. 1(a), the feeding probe imposes an electrical perturbation and induces weakly coupled TM_{02} mode. TM_{10} is the primary radiating mode, estimated by the equivalent magnetic currents $\mathbf{M_1}$ and $\mathbf{M_1'}$ [Fig. 1(b)] whereas $\mathbf{M_2}$, $\mathbf{M_2'}$, $\mathbf{M_3}$, and $\mathbf{M_3'}$ do not contribute to radiation. But $\mathbf{M_4}$ and $\mathbf{M_4'}$ [Fig. 1(a)] cause radiation due to TM_{02} (primary XP source over the H-plane [2]) and may be expressed as

$$\mathbf{M_4'} = -\mathbf{M_4'} = 2E_0\hat{x} \tag{1}$$

where E_0 is the maximum electric field across *ps* and *qr*.

$\mathbf{M_4'} = -\mathbf{M_4'}$ induced far radiation fields are derived as [1]

$$E_\theta = E_0\, Lh \frac{jke^{-jkr}}{2\pi r} \{\sin(\varphi)\,\mathrm{sinc}(X)\,\mathrm{sinc}(Z)\} \tag{2}$$

This work was supported by the Scheme of Abdul Kalam Technology Innovation National Fellow of the Indian National Academy of Engineering/ Department of Science and Technology-Science and Engineering Research Board (INAE/DST-SERB), Government of India. *(Corresponding author: Sk Rafidul)*

Sk Rafidul is with the Institute of Radio Physics and Electronics, University of Calcutta, Kolkata 700009, India (e-mail: rafidul100@gmail.com).

Mobayode O. Akinsolu is with the Faculty of Arts, Computing, and Engineering, Wrexham University, LL11 2AW Wrexham, U.K.

Bo Liu is with the James Watt School of Engineering, University of Glasgow, G12 8QQ Glasgow, U.K.

Chandrakanta Kumar is with the Communication Systems Group, U R Rao Satellite Centre, Department of Space, Government of India, Bangalore 560017, India.

Debatosh Guha is with the Institute of Radio Physics and Electronics, University of Calcutta, Kolkata 700009, India, and also with the Department of Electronics and Communication Engineering, National Institute of Technology, Jaipur 302017, India.

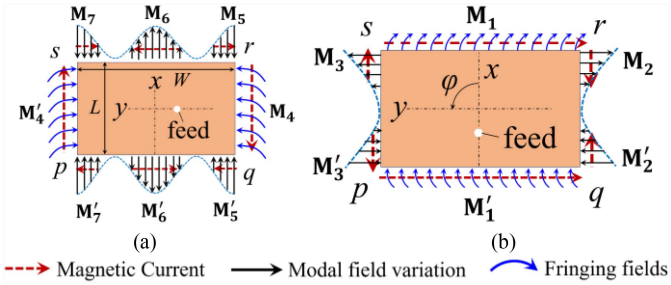

Fig. 1. Modal field and magnetic current distribution around the patch *pqrs*, (a) TM_{02} mode. (b) TM_{10} mode.

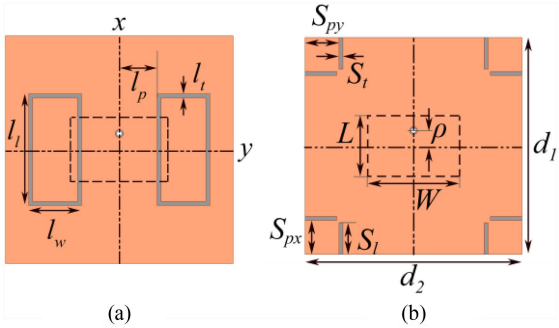

Fig. 2. Rectangular patch with ground bearing. (a) Config I: loops. (b) Config II: slots.

$$E_\varphi = E_0\, Lh \frac{jke^{-jkr}}{2\pi r} \{\cos(\theta)\cos(\varphi)\,\mathrm{sinc}(X)\,\mathrm{sinc}(Z)\} \quad (3)$$

with $X = \frac{kL}{2}\sin\theta\cos\varphi$ and $Z = \frac{kh}{2}\cos\theta$.

Here, k is the wavenumber, θ and φ are elevation and azimuth angles, respectively, and h is the slot height. $\mathbf{M_4}$ and $\mathbf{M'_4}$ form a 2-element array with an array factor $A_F = 2\sin(\frac{kW}{2}\sin(\theta)\sin(\varphi))$ and results in H-plane fields as

$$E_{\theta|\mathrm{total}} = \frac{jke^{-jkr}}{\pi r}\left\{\mathrm{sinc}\left(\frac{kh}{2}\cos\theta\right)\right\}\left\{\sin\left(\frac{kW}{2}\sin\theta\right)\right\} \quad (4)$$

$$E_{\varphi|\mathrm{total}} = 0. \quad (5)$$

Significant radiations from *ps* and *qr* are apparent and, therefore, magnetic currents $\mathbf{M_4}$ and $\mathbf{M'_4}$ need to be reduced. Based on gathered knowledge through [13], [14], [15], [16], and [17], a defect has been strategically deployed underneath each fringing area with a view to weakening TM_{02} mode. Here, it is conceived as a resonant rectangular loop of dimension $\sim\lambda_0$ [Fig. 2(a): Config I]. The full-wavelength electric fields trapped within the loop would eventually cause no leakage or radiation.

However, we learned that the weakening of TM_{02} mode hardly caused any improvement in D-plane XP [9]. A further study [18] gave more insights and established conduction currents around the GP corners as a major source for D-plane XP radiations. Based on this understanding, some innovative engineering around the GP corners has been introduced. The scheme is shown in Fig. 2(b): Config II. It embodies a pair of mutually orthogonal slits. They favorably reorient the current vectors around the slits to produce an effectively null conduction current. Related physical insights are discussed in Section IV.

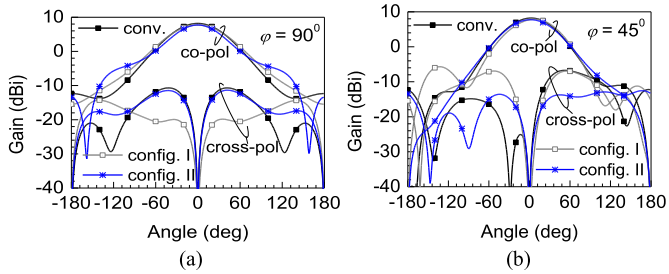

Fig. 3. Radiation patterns for different GP configurations at $f = 5.75$ GHz, (a) H-plane, (b) D-plane. Parameters: $L = 15.5$, $W = 23.25$, $\rho = 3.9$, $l_p = 12$, $l_l = 18$, $l_w = 7$, $l_t = 0.5$, $S_l = 8$, $S_w = 1$, $S_{px} = 8.6$, $S_{py} = 8.6$, $d_1 = d_2 = 52$, substrate thickness $h = 1.575$, $\varepsilon_r = 2.33$. All parameters are in mm.

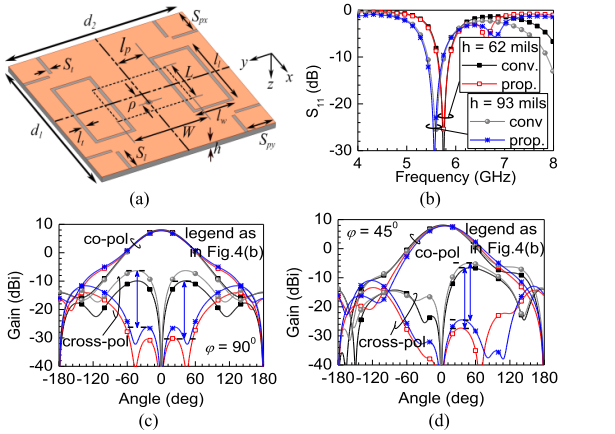

Fig. 4. DGG integrated rectangular patch with varying h: (a) ground geometry, (b) simulated S_{11}, (c) H-plane pattern, and (d) D-plane pattern. $L = 15.5$ mm, $W = 23.25$ mm, $\varepsilon_r = 2.33$. The rest of the parameters were optimized for each h value.

The built-in PSO algorithm of [29] has been used to optimize the parameters associated with each of the configurations, individually. Achieving the minimum XP level without any degradation in the peak gain has been the basis of optimization. The simulated results are compared in Fig. 3. As conjectured, Config I excels in suppressing H-plane XP. Conversely, Config II demonstrates greater efficacy in mitigating D-plane XP.

Thus, Configs I and II together should handle both D- and H-planes issues. Keeping this in view, we propose a new multi-parametric DGG as in Fig. 4(a). Optimization of the same was tried with the PSO algorithm, but it failed. A more advanced technique (i.e., PSADEA) has been explored and discussed.

III. PSADEA-Based Optimization and Results

The PSADEA [22], [23], the third installment of the SADEA series of algorithms [24], suits challenging antenna design cases requiring high-quality solutions (e.g., [25], [26]). The supervised learning technique, in PSADEA, is a Gaussian process, and the evolutionary computation technique is DE. One of the key advantages is its ability to function without the need for a good-quality initial design or ad-hoc process.

It follows a few steps and to initiate the optimization process, the design space of the proposed DGG is sampled using Latin hyper-cube sampling [27] to generate a small number of designs. The designs and their simulated results are used to create the initial database. Iteratively, offspring solutions

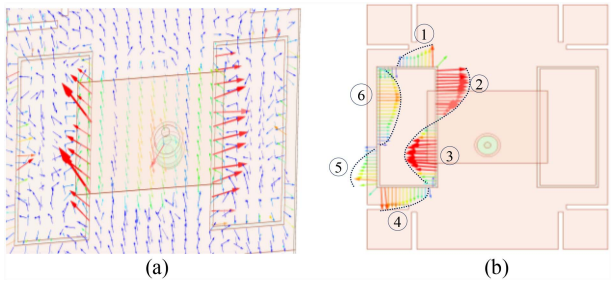

Fig. 5. (a) Substrate electric field due to TM_{02} mode for the proposed GP. Parameters as in Fig. 4 with $\rho = 2.5$ mm along y-direction, (b) variation of electric fields within the loop at the resonant frequency of TM_{10} mode. Parameters as in Fig. 4.

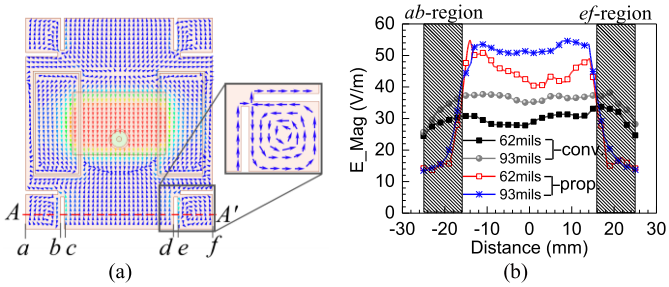

Fig. 6. (a) GP surface current distribution in proposed GP. (b) Magnitude of near-electric field variation over a line AA′ located on the surface of the substrate as shown in (a). Parameters as in Fig. 4.

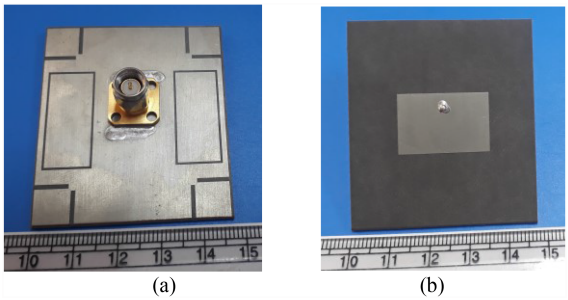

Fig. 7. Fabricated prototypes of the proposed antenna for rectangular patch element. (a) Back view. (b) Top view. Parameters as in Fig. 4 with $\rho = 4.03$, $d_1 = 52.45$, $d_2 = 46.04$, $l_l = 25.43$, $l_w = 10.55$, $l_t = 0.78$, $l_p = 10.22$, $S_l = 7.93$, $S_w = 1.29$, $S_{px} = 8.53$, $S_{py} = 8.49$.

are created by applying three DE mutation operators self-adaptively on the top τ candidate design solutions. For each of them, Gaussian process-based surrogate models are built using the nearest (based on Euclidean distance) designs from the database and their performance values as the training data points. The resulting offspring solutions are then prescreened to handle prediction uncertainty using the lower confidence bound (LCB) approach [28]. The chosen top solutions (three in this case) are then simulated concurrently and added to the database alongside their simulation results. More details are available in [22] and [23].

For the present structure, shown in Fig. 4(a) with any standard patch shape, the population size is considered to be 50 and the parametric search ranges cum constraints are predetermined (not shown in detail). Other algorithmic parameter settings are as [22] and [23]. The optimization goal is to achieve $\max|S_{11}| \leq -20$ dB at the C-band frequency, $G_{\text{peak}} \geq 7.7$ dBi, peak XP

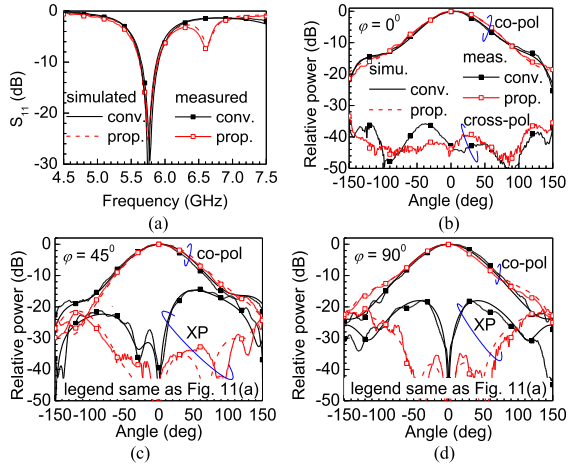

Fig. 8. (a) Measured S_{11} of the rectangular patch bearing proposed and conventional ground. Radiation patterns of the rectangular patch measured at $f = 5.75$ GHz for the proposed GP and $f = 5.77$ GHz for conventional GP compared with their simulated predictions: (b) E-plane, (c) D-plane, and (d) H-plane. Parameters as in Fig. 4.

over D-plane ($\varphi = 45°$; $-60° \leq \theta \leq +60°$), $D_{\text{xp}} < -28$ dB, and a peak XP over H-plane ($\varphi = 90°$; $-60° \leq \theta \leq +60°$), $H_{\text{xp}} < -32$ dB, by minimizing the cost function (Q) as follows:

$$\begin{aligned} Q = w_1 \times \{&\max([|S_{11}| + 20\text{ dB}, 0]) + \max([G_{\text{TH}} \\ &- G_{\text{peak}}, 0]) + \max([G_{\text{cop}} + 10\text{ dBi}, 0])\} \\ &+ w_2 \times \{\max([D_{\text{xp}} + 28\text{ dB}, 0]) \\ &+ \max([H_{\text{xp}} + 32\text{ dB}, 0])\} \end{aligned} \tag{6}$$

with $w_1 = 50$ and $w_2 = 1$ allowing the optimization process to preferentially ensure that S_{11} and G_{peak} specifications are firstly met, before focusing on satisfying the D_{xp} and H_{xp} specifications. G_{TH} is considered to be 7.7 dBi and Q becomes zero when all the specifications are achieved. Our process successfully achieved DGG designs for rectangular, circular, and square patches with $Q = 0$, using 1310, 1324, and 1296 electromagnetic (EM) simulations, respectively, within 4 days on average. The same cases by PSO from [29] result in $Q = 428$ after 4581 EM simulations, which took over two weeks to complete.

The working stability of the current DGG design is evaluated by selecting two different patch geometries for optimization. Following the successful optimization of the DGG for two different substrate heights using the PSADEA method, the results are analyzed and compared with their conventional version, as shown in Fig. 4(b)–(d). The resonant frequency remains unaltered except in revealing a second deep in the S_{11} [Fig. 4(b)]. This may be attributed to the resonant loops on the GP, to be discussed in Section IV.

The H- and D-plane radiation patterns [Fig. 4(c)–(d)] promise about 20 dB XP suppression in each plane, although their copolarization radiations remain mutually consistent. Eventually, it results in about 35 dB co-to-XP isolation consistently over all radiation planes. This, indeed is an extraordinary achievement reported here for the first time.

TABLE I
PROPOSED WORK COMPARED WITH SOME RELEVANT REPORTED WORK

Previous works		Freq. band	XP suppression (dB)		Peak Gain (dBi)	% BW	Comments
			D-plane	H-plane			
[19]		S	10	13	7.0	1.9	Difficulty in array implementation. Peak gain is reduced. Performance is not satisfactory
[20]		S	11 $12^{\$,@@}$	0 $\uparrow 5^{\$,@@}$	7.8 $10^{@@}$	3.4 $2.4^{@@}$	
[21]		C	7	0	9.1	2.9	
[14]		X	#	18	6.2	6.3	Effective over H-plane. D-plane performance is not satisfactory
[10]		L	8	25	9.1	1.3	
Present	single	C	18	18	8.0	5	Simple design and fabrication. Effective over all φ planes for all commonly used patch shapes, and arrays
	array		13	13	12.6	3.4	

not shown, $ no measured data, ↑ indicates increment, @@ indicates array

IV. DESIGN PHYSICS AND INTERPRETATION

Initially, it was believed that the loop perimeter needs to be approximately of the order of λ_0 to interact with TM_{02} mode and make it weaker. However, the AI-generated results reveal that the optimized value is $\{2(l_l\text{-}l_t)+2(l_w\text{-}l_t)\} = 2\lambda_g$. The insight into the same has been developed with the help of simulated portrays for TM_{02} mode [Fig. 5(a)]. The fringing fields get trapped within the DGG. The same DGG with TM_{10} mode is examined in Fig. 5(b). It is apparent that the fields get coupled to the loop to form two complete full-wave variations. Specifically, the variations ①, ②, and ③ together form one full cycle, while ④, ⑤, and ⑥ constitute another full-wave variation. Therefore, the loop defects become safe as they effectively produce no hazardous leakage or unwanted radiation.

The contribution of the corner defects has been examined in Fig. 6. The blow-up picture in Fig. 6(a) shows the nature of the conduction current which gets modified by the corner defects. It reveals an effective null around the corners for both substrate heights. This pictorial observation has been confirmed by comparing the near electric fields [Fig. 6(b)] across a line AA' (lies on the substrate). This illustration demonstrates that the electric field within the regions labeled '*ab*' and '*ef*' experiences a significant decrement. This eventually results in a major suppression across the D-plane.

V. EXPERIMENT AND VERIFICATION

A pair of C-band prototypes, bearing a conventional ground geometry and the proposed GP has been fabricated on a Rogers RT/Duroid 5870 substrate with a relative permittivity of 2.33, as shown in Fig. 7. Radiall SMA connectors have been used for the feeding. The S_{11} patterns were measured using an E8363B precision network analyzer, while the far-field measurements were carried out in an anechoic chamber equipped with an MI-750 microwave receiver.

The measured S_{11} depicted in Fig. 8(a) is in perfect agreement with the simulated predictions. The radiation patterns are shown in Fig. 8(b)–(d). The measurements closely corroborate the simulated data and ensure as much as 18 dB suppression in XP fields over both D- and H-planes. The E-plane XP consistently lies below −35 dB. The proposed antenna exhibits a measured peak gain of around 8.0 dBi. This provided an overall co-to-XP isolation of about 33 dB over the entire radiation plane.

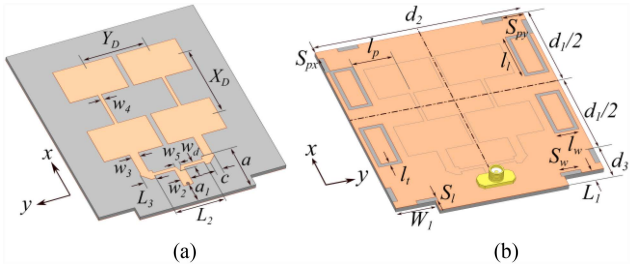

Fig. 9. Geometry of the 2 × 2 proposed array. (a) Top view. (b) Bottom view.

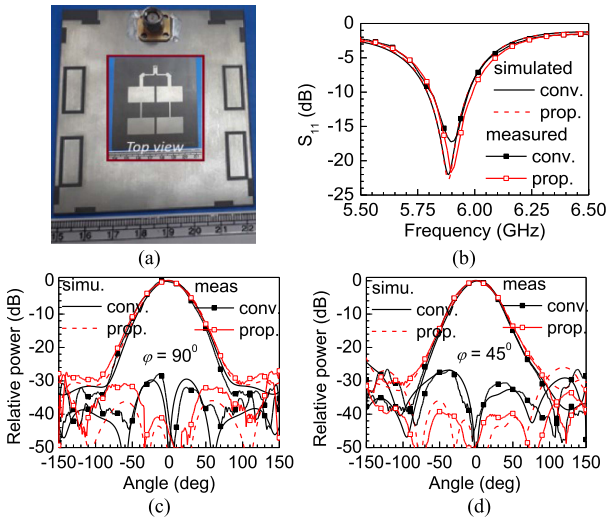

Fig. 10. (a) Prototype of the fabricated 2 × 2 proposed array. Measured and simulated (b) S_{11}, (c) H-plane pattern, and (d) D-plane pattern. Parameters: $D_1 = 71$, $D_2 = 74$, $D_3 = 16$, $X_D = 30.2$, $Y_D = 25.3$, $w_4 = 1.3$, $L_2 = 19.5$, $w_2 = 3.8$, $w_3 = 3.3$, $w_5 = 2.7$, $w_d = 2.4$, $a = 19$, $a_1 = 7.8$, $c = 2.9$, $L_1 = 4.8$, $W_1 = 14.1$, $l_l = 20.7$, $l_w = 8.6$, $l_t = 1.4$, $l_p = 14.5$, $s_l = 1.8$, $s_w = 7.3$, $S_{px} = 3.3$, $S_{py} = 7.7$. All parameters are in mm.

A 2 × 2 array (Fig. 9) is examined to ensure the design viability. Unlike some earlier cases [18], [19], [20], [21], the present DGG is found to be effective. The measured results are shown in Fig. 10, where measured S_{11} closely corroborates the simulated prediction. Its far-field patterns ensure nearly 13 dB XP suppression over both D- and H-planes with a peak gain of 12.5 dBi. A further increase in array elements (say, 4 × 4) is also viable, with the proposed DGG configuration revealing about 4.5 dB increase in peak gain (relative to the 2 × 2 array version). But the order of XP suppression gets reduced from 13 dB (2 × 2 array) to 7 dB (4 × 4 array).

VI. CONCLUSION

This multiparametric defected ground design appears versatile as it stands valid for different varying patch geometries as well as arrays without creating any feed deployment issues, even in the presence of a radome tested with polymethacrylimide based Rohacell ($\varepsilon_r = 1.09$) material. Table I provides a useful comparison with some earlier relevant designs. A few recent studies [10], [18], [19], [20], [21] focused on D-plane XPs. However, [10] and [19] appear unsuitable for array platforms due to feed deployment issues, [20] becomes less sensitive to H-plane, and [21] fails in addressing D-plane adequately. The present design significantly surpasses those earlier works and offers significant 3-D XP improvement.

REFERENCES

[1] C. A. Balanis, *Antenna Theory: Analysis and Design*, 4th ed. New York, NY, USA: Wiley, 2016.

[2] D. Guha, C. Kumar, and S. Biswas, *Defected Ground Structure (DGS) Based Antennas*, 1st ed. New York, NY, USA: Wiley, 2022.

[3] R. Hansen, "Cross polarization of microstrip patch antennas," *IEEE Trans. Antennas Propag.*, vol. AP-35, no. 6, pp. 731–732, Jun. 1987.

[4] C.-Y.-D. Sim, C.-C. Chang, and J.-S. Row, "Dual-feed dual-polarized patch antenna with low cross polarization and high isolation," *IEEE Trans. Antennas Propag.*, vol. 57, no. 10, pp. 3405–3409, Oct. 2009.

[5] A. Petosa, A. Ittipiboon, and N. Gagnon, "Suppression of unwanted probe radiation in wideband probe-fed microstrip patches," *Electron. Lett.*, vol. 35, no. 5, pp. 355–357, Mar. 1999.

[6] H.-W. Lai and K.-M. Luk, "Design and study of wide-band patch antenna fed by meandering probe," *IEEE Trans. Antennas Propag.*, vol. 54, no. 2, pp. 564–571, Feb. 2006.

[7] Z. Shao, L.-F. Qiu, and Y. P. Zhang, "Design of wideband differentially fed multilayer stacked patch antennas based on bat algorithm," *IEEE Antennas Wireless Propag. Lett.*, vol. 19, no. 7, pp. 1172–1176, Jul. 2020.

[8] S. Chakraborty, A. Ghosh, S. Chattopadhyay, and L. L. K. Singh, "Improved cross-polarized radiation and wide impedance bandwidth from rectangular microstrip antenna with dumbbell-shaped defected patch surface," *IEEE Antennas Wireless Propag. Lett.*, vol. 15, pp. 84–88, 2016.

[9] C. Kumar and D. Guha, "Higher mode discrimination in a rectangular patch: New insight leading to improved design with consistently low cross-polar radiations," *IEEE Trans. Antennas Propag.*, vol. 69, no. 2, pp. 708–714, Feb. 2021.

[10] Z. Shao and Y. Zhang, "Cross-polarization reduction of shorted patch antenna by using coupled $TM_{0,1/2}$ mode," *IEEE Trans. Antennas Propag.*, vol. 69, no. 12, pp. 8115–8124, Dec. 2021.

[11] K.-L. Wong, C.-L. Tang, and J.-Y. Chiou, "Broadband probe-fed patch antenna with a W-shaped ground plane," *IEEE Trans. Antennas Propag.*, vol. 50, no. 6, pp. 827–831, Jun. 2002.

[12] G. H. Huff and J. T. Bernhard, "Improvements in the performance of microstrip antennas on finite ground planes through ground plane edge serrations," *IEEE Microw. Wireless Compon. Lett*, vol. 12, no. 8, pp. 308–310, Aug. 2002.

[13] D. Guha, M. Biswas, and Y. M. M. Antar, "Microstrip patch antenna with defected ground structure for cross polarization suppression," *IEEE Antennas Wireless Propag. Lett.*, vol. 4, pp. 455–458, 2005.

[14] C. Kumar and D. Guha, "Reduction in cross-polarized radiation of microstrip patches using geometry-independent resonant-type defected ground structure (DGS)," *IEEE Trans. Antennas Propag.*, vol. 63, no. 6, pp. 2767–2772, Jun. 2015.

[15] D. K. Naik, R. Swain, D. C. Panda, and R. K. Mishra, "CMA approach for a DGS-based wideband circular patch antenna with low cross polarization," *IEEE Antennas Wireless Propag. Lett.*, vol. 22, no. 3, pp. 586–590, Mar. 2023.

[16] B. Qian, X. Chen, L. Zhao, J. Chen, and A. A. Kishk, "Reduced cross-polarization and backside radiations for rectangular microstrip antennas using defected ground structure combined with decoupling structure," *IEEE Antennas Wireless Propag. Lett.*, vol. 22, no. 3, pp. 517–521, Mar. 2023.

[17] A. Ghosh, D. Ghosh, S. Chattopadhyay, and L. L. K. Singh, "Rectangular microstrip antenna on slot-type defected ground for reduced cross-polarized radiation," *IEEE Antennas Wireless Propag. Lett.*, vol. 14, pp. 321–324, 2015.

[18] M. I. Pasha, C. Kumar, and D. Guha, "Mitigating high cross-polarized radiation issues over the diagonal planes of microstrip patches," *IEEE Trans. Antennas Propag.*, vol. 68, no. 6, pp. 4950–4954, Jun. 2020.

[19] D. Dutta, S. Rafidul, D. Guha, and C. Kumar, "Suppression of cross-polarized fields of microstrip patch across all skewed and orthogonal radiation planes," *IEEE Antennas Wireless Propag. Lett.*, vol. 19, no. 1, pp. 99–103, Jan. 2020.

[20] D. Dutta, D. Guha, and C. Kumar, "A concept of advanced design governed by theoretically predicted current distributions on the ground plane beneath an aperture-fed microstrip antenna," *IEEE Open J. Antennas Propag.*, vol. 4, pp. 461–471, 2023.

[21] S. Rafidul, C. Kumar, and D. Guha, "A technique to realize aperture coupled microstrip patch as a truly low cross-polar antenna by mitigating the major issues over its skewed radiation planes," *IEEE Open J. Antennas Propag.*, vol. 4, pp. 754–763, 2023.

[22] M. O. Akinsolu, B. Liu, V. Grout, P. I. Lazaridis, M. E. Mognaschi, and P. D. Barba, "A parallel surrogate model assisted evolutionary algorithm for electromagnetic design optimization," *IEEE Trans. Emerg. Topics Comput. Intell.*, vol. 3, no. 2, pp. 93–105, Apr. 2019.

[23] B. Liu et al., "Efficient global optimisation of microwave antennas based on a parallel surrogate model-assisted evolutionary algorithm," *Microw., Antennas Propag.*, vol. 13, no. 2, pp. 149–155, 2019.

[24] Y. Liu et al., "An efficient method for antenna design based on a self-adaptive Bayesian neural network-assisted global optimization technique," *IEEE Trans. Antennas Propag.*, vol. 70, no. 12, pp. 11375–11388, Dec. 2022.

[25] J. Zhang, M. O. Akinsolu, B. Liu, and S. Zhang, "Design of zero clearance SIW endfire antenna array using machine learning-assisted optimization," *IEEE Trans. Antennas Propag.*, vol. 70, no. 5, pp. 3858–3863, May 2022.

[26] Q. Zheng, C. Guo, J. Ding, M. O. Akinsolu, B. Liu, and G. A. E. Vandenbosch, "A wideband low-RCS metasurface-inspired circularly polarized slot array based on AI-driven antenna design optimization algorithm," *IEEE Trans. Antennas Propag.*, vol. 70, no. 9, pp. 8584–8589, Sep. 2022.

[27] M. Stein, "Large sample properties of simulations using Latin hypercube sampling," *Technometrics*, vol. 29, pp. 143–151, 1987.

[28] M. T. M. Emmerich, K. C. Giannakoglou, and B. Naujoks, "Single- and multiobjective evolutionary optimization assisted by Gaussian random field metamodels," *IEEE Trans. Evol. Computation*, vol. 10, no. 4, pp. 421–439, Aug. 2006.

[29] "CST Microwave StudioR 2021," 2021. [Online]. Available: https://www.3ds.com/products/simulia/cst-studio-suite